Effects of internal mineral structures on the magnetic remanence of silicate-hosted titanomagnetite inclusions: An electron holography study

Joshua M. Feinberg,[1] Richard J. Harrison,[1] Takeshi Kasama,[2,3] Rafal E. Dunin-Borkowski,[2,3] Gary R. Scott,[4] and Paul R. Renne[4,5]

Received 10 May 2006; revised 12 October 2006; accepted 26 October 2006; published 30 December 2006.

[1] Titanomagnetite inclusions in pyroxene and plagioclase are carriers of stable magnetic remanence in some slowly cooled rocks such as gabbros, anorthosites, granulites, and diorites. Needle-shaped inclusions with average dimensions of $1 \times 1 \times >25$ μm form epitaxially by exsolution from their host silicate. Close examination of clinopyroxene-hosted inclusions reveals an internal microstructure, which consists of magnetite (Fe_3O_4) prisms and ulvöspinel (Fe_2TiO_4) lamellae that formed as a result of phase unmixing during initial cooling. This internal structure exerts a profound influence on the magnetic remanence properties of each inclusion, primarily by transforming it from a multidomain grain into an assemblage of magnetostatically interacting single-domain prisms. Here we use off-axis electron holography to image the magnetization states of individual prisms and the magnetostatic interactions between them. We show that the inclusions exhibit both single-domain and collective magnetic states that depend primarily on the shape anisotropies of individual magnetite prisms, magnetostatic interactions between closely spaced prism stacks, and the shape anisotropy of the needle itself. Prisms that are separated by thick ulvöspinel lamellae show uniformly magnetized and/or vortex states. In contrast, closely spaced magnetite prisms behave as multipart vortices or as long composite columns, whose strong net magnetization may not be related directly to the orientation and shape of either the needle or the constituent prisms. The overall remanence direction recorded by clinopyroxene crystals containing finely exsolved inclusions is a reflection of both the inclusions' elongation directions and the prism arrangements within them.

Citation: Feinberg, J. M., R. J. Harrison, T. Kasama, R. E. Dunin-Borkowski, G. R. Scott, and P. R. Renne (2006), Effects of internal mineral structures on the magnetic remanence of silicate-hosted titanomagnetite inclusions: An electron holography study, *J. Geophys. Res.*, *111*, B12S15, doi:10.1029/2006JB004498.

1. Introduction

[2] Rock magnetic recorders that are stable with respect to variations in temperature, pressure and redox conditions are needed to expand the coverage of the paleomagnetic timescale into the Paleozoic and Precambrian, and to gather information about the direction and intensity of the Earth's ancient magnetic field. Occluded magnetic inclusions in single crystals of plagioclase have recently been developed as reliable paleomagnetic recorders [*Cottrell and Tarduno*, 1999, 2000; *Tarduno et al.*, 2001, 2002; *Smirnov et al.*, 2003; *Tarduno and Cottrell*, 2005]. Exsolved magnetic inclusions in common silicate minerals such as plagioclase and pyroxene (Figure 1) have demonstrated considerable promise for pre-Mesozoic paleomagnetic studies for over 40 years and are characterized by high median destructive fields (>80 mT), high unblocking temperatures (>530°C), and univectorial remanence during alternating field and thermal demagnetization experiments [*Evans and McElhinny*, 1966; *Evans et al.*, 1968; *Hargraves and Young*, 1969; *Murthy et al.*, 1971; *Wu et al.*, 1974; *Davis*, 1981; *Scofield and Roggenthen*, 1986; *Hattingh*, 1986a; 1986b, 1989; *Renne and Onstott*, 1988; *Schlinger and Veblen*, 1989; *Bogue et al.*, 1995; *Halls and Zhang*, 1995; *Xu et al.*, 1997; *Hargraves et al.*, 1999; *Selkin et al.*, 2000; *Yu and Dunlop*, 2001; *Renne et al.*, 2002; *Feinberg et al.*, 2005]. Although the remanence of bulk samples containing these inclusions matches expected field directions in cases where the latter are known [*Bogue et al.*, 1995; *Renne et al.*, 2002],

[1]Department of Earth Sciences, University of Cambridge, Cambridge, UK.
[2]Department of Materials Science and Metallurgy, University of Cambridge, Cambridge, UK.
[3]Frontier Research System, Institute of Physical and Chemical Research, Hatoyama, Japan.
[4]Berkeley Geochronology Center, Berkeley, California, USA.
[5]Department of Earth and Planetary Science, University of California, Berkeley, California, USA.

0148-0227/06/2006JB004498$09.00

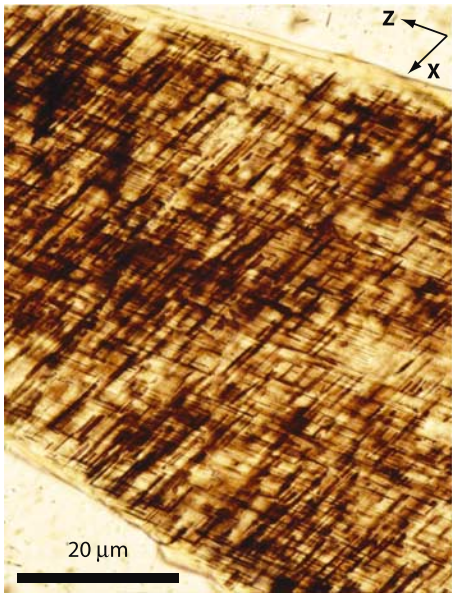

Figure 1. Photomicrograph of crystallographically oriented magnetite inclusions in clinopyroxene from the Messum Complex. Two orientations of inclusions are parallel to the (010) of clinopyroxene. One set is elongated subparallel to $[001]_{cli}$ (Z inclusions), while the other is elongated subparallel to $[100]_{cli}$ (X inclusions). The magnetic remanence recorded by a single crystal of clinopyroxene always occurs within the $(010)_{cli}$ plane.

several questions about the origin of remanence in silicate-hosted magnetic inclusions preclude their immediate use as paleomagnetic recorders. In particular, if silicate-hosted magnetic inclusions are to be used in paleomagnetic studies, then it is necessary to determine whether their internal microstructures affect the accuracy of the recorded magnetic direction and intensity. Here, we address experimentally the effects of intrainclusion microstructures on the direction and intensity of remanence associated with such inclusions.

2. Sample Description

[3] This study examines clinopyroxene crystals containing crystallographically oriented titanomagnetite inclusions from the 132 Ma Messum Volcanic Complex of Namibia whose average compositions are $Wo_{46}En_{44}Fs_{10}$ to $Wo_{45}En_{43}Fs_{12}$ [*Feinberg et al.*, 2004]. The inclusions formed initially at 825 ± 25°C as homogeneous needles of titanomagnetite solid solution ($Fe_{3-x}Ti_xO_4$) within their silicate host [*Feinberg et al.*, 2004]. In some clinopyroxene crystals, two elongation directions of needles are present: one subparallel to the clinopyroxene's *a* axis, and the other subparallel to the clinopyroxene *c* axis (termed "X" and "Z" inclusions, respectively, by *Fleet et al.* [1980]). Occasionally, one inclusion orientation (usually the Z) is dominant within a single crystal. The host gabbro containing the clinopyroxene crystals cooled under a minimum rate of 1000°C/Ma [*Renne et al.*, 2002] and proceeded at an oxygen fugacity (fO_2) below the hematite-magnetite buffer. During this initial cooling the clinopyroxene-hosted inclusions unmixed to form nanometer-scale intergrowths of nearly pure magnetite (Fe_3O_4) and ulvöspinel (Fe_2TiO_4). The formation of this intrainclusion microtexture (Figure 2) dramatically alters the inclusions' magnetic remanence properties by subdividing each would-be multidomain crystal into an assemblage of interacting single-domain magnetite prisms [*Evans and Wayman*, 1974; *Feinberg et al.*, 2005; *Evans et al.*, 2006]. Although ubiquitous in the inclusions of the Messum Complex, not all silicate-hosted magnetic inclusions exhibit this magnetite-ulvöspinel texture. The presence of this texture is likely a reflection of the original Ti content of the host silicate, fO_2, and cooling rate.

3. Experimental Details

3.1. Rock Magnetic Experiments

[4] Hysteresis measurements were performed on a Princeton MicroMag 2900 alternating gradient magnetometer at the Paleomagnetism Laboratory at the University of California, Davis. Isothermal remanent magnetization acquisition and back-field demagnetization experiments were conducted using an ASC impulse magnetizer and a 2G-755R cryogenic magnetometer at the Berkeley Geochronology Center's Paleomagnetism Laboratory.

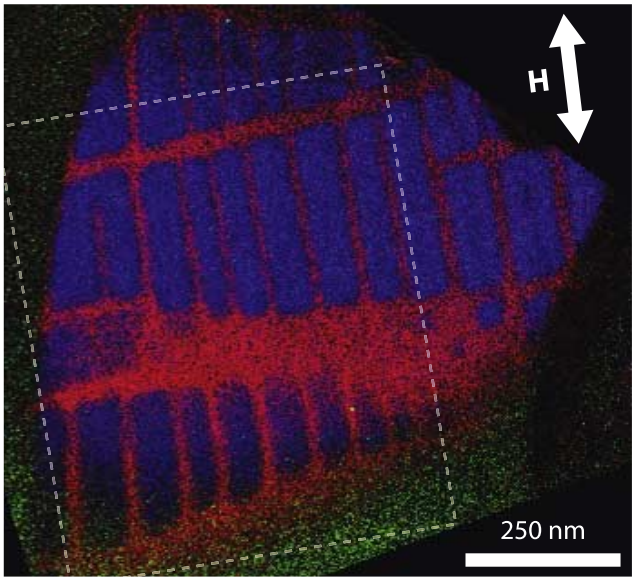

Figure 2. Chemical map, acquired using three-window background-subtracted elemental mapping with a Gatan imaging filter, showing a crystallographically oriented magnetite inclusion exsolved in clinopyroxene from the Messum Complex, Namibia. Blue, red, and green represent enrichment in iron (magnetite), titanium (ulvöspinel), and calcium (clinopyroxene), respectively. The double-headed arrow denotes the direction of the in-plane component of the magnetic field applied to the sample before acquiring the holograms used to record Figures 6 and 7. The dashed box represents the area used to calculate the coercivity of remanence in Figure 7.

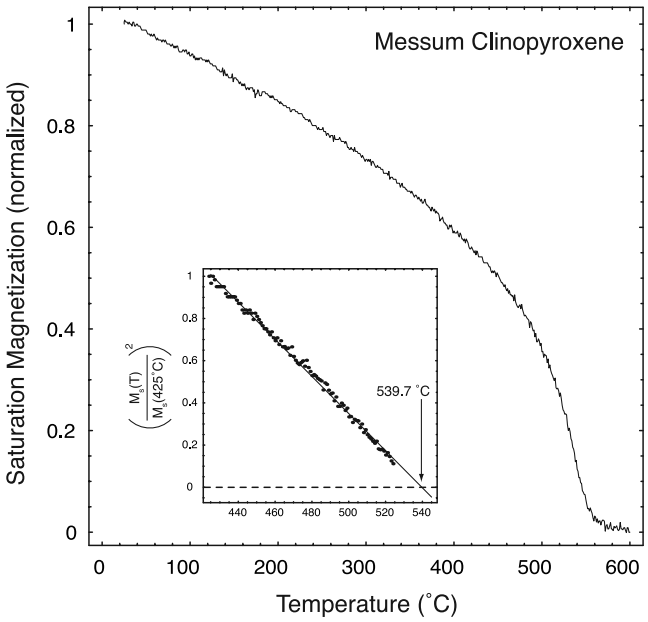

Figure 3. Thermomagnetic curve for a Messum clinopyroxene containing inclusions with magnetite-ulvöspinel intergrowths. Both the extrapolated method of *Moskowitz* [1981] (see inset) and the differential method of *Tauxe* [1998] yield Curie temperatures of 540°C.

Strong-field thermomagnetic curves were measured (at 1.5 T) using the Princeton Measurements vibrating sample magnetometer at the Institute for Rock Magnetism at the University of Minnesota.

3.2. Electron Microscopy

[5] Clinopyroxene crystals were extracted from a standard petrographic thin section and prepared for transmission electron microscopy (TEM) using mechanical polishing and argon ion-beam milling. Areas of the completed TEM specimen that were most suitable for electron holography (close to the tapered edge) contained needle-shaped inclusions oriented with their long axes roughly normal to the sample surface. TEM observations were carried out at 300 kV using a Philips Electron Optics (Eindhoven, Netherlands) CM300-ST TEM equipped with a field emission gun, a Lorentz lens, an electrostatic biprism and a Gatan (Pleasanton, California) imaging filter. Energy-selected imaging [*Egerton*, 1996; *Golla and Putnis*, 2001] was used to measure the compositions of the inclusions and the clinopyroxene host. Off-axis electron holography [*Tonomura*, 1992; *Völkl et al.*, 1998] was used to provide maps of the in-plane magnetic induction in the samples with ~10 nm spatial resolution (see below). Digital acquisition and analysis of the electron holograms allowed the magnetic signal of primary interest to be separated from unwanted contributions to the contrast and from variations in specimen thickness and mean inner potential [*Dunin-Borkowski et al.*, 2004].

[6] Remanent magnetic states in the inclusion shown in Figure 2 were studied using methods similar to those described by *Harrison et al.* [2002]. Prior to each measurement, the sample was tilted by an angle of plus or minus 30° to the horizontal and exposed for 1–2 s to the 2 T vertical field of the TEM objective lens. The saturation isothermal remanent magnetization (SIRM) obtained is that which results after the sample's magnetization (which is initially out of plane) relaxes into the plane of the TEM sample. Next, the sample was tilted by 30° in the opposite direction (in zero field) and exposed to a smaller magnetic field in order to impart an IRM antiparallel to the initial SIRM. Finally, the sample was tilted back to 0° in zero field for characterization of the resulting remanent states. Ten different objective lens currents were used to generate IRM fields of 0, 10.1, 24.7, 30.1, 40.8, 51.5, 62.2, 72.9, 83.5, and 104.9 mT.

4. Results

4.1. Rock Magnetism

[7] A strong-field thermomagnetic curve from a representative sample of Messum clinopyroxene containing finely exsolved inclusions is shown in Figure 3. Both the extrapolation method of *Moskowitz* [1981] and the differential method of *Tauxe* [1998] yield Curie points of 540°C, which corresponds to an oxide composition of $Fe_{2.93}Ti_{0.07}O_4$ [*Akimoto*, 1962]. Hysteresis loops of individual silicate crystals containing magnetic inclusions are highly sensitive to the orientation of the applied field. Figure 4a shows a hysteresis loop from a Messum clinopyroxene collected with the applied field parallel to the crystallographic plane containing both sets of inclusions' $(010)_{cli}$ and perpendicular to the clinopyroxene c axis. Values for the saturation remanence magnetization (M_R) and saturation magnetization (M_S) are 0.78×10^{-7} A m^2 and 1.05×10^{-7} A m^2, respectively. Values for the coercivity of remanence (H_{CR}) and bulk coercivity (H_C) are 108 mT and 95 mT, respectively. These hysteresis parameters give M_R/M_S and H_{CR}/H_C ratios of 0.74 and 1.14; values normally ascribed to single-domain materials. Bulk rock samples display similarly hard coercivities. Figure 4b shows coercivity spectra from single crystal IRM acquisition and back-field demagnetization experiments. The IRM acquisition curve flattens out shortly after 300 mT, consistent with a low-Ti titanomagnetite.

[8] The back-field demagnetization curve shown in Figure 4b was projected onto the IRM acquisition curve in two ways. First, by reflecting and rescaling the back-field demagnetization curve into the forward field, it is possible to observe its crossover with the IRM acquisition curve. A second, inverted projection of the back-field demagnetization curve is included to allow direct comparison of the acquisition and demagnetization of DC magnetic fields [*Dunlop*, 1986]. An assemblage of noninteracting single-domain grains would show a crossover point or R value close to 0.5 M_{rs} and a consistent point-to-point match between the IRM acquisition and back-field demagnetization curves. The clinopyroxene crystal in Figure 4b has a crossover R value <0.5 M_{rs} and the inverted back-field demagnetization curve differs from the IRM acquisition curve. As pointed out by *Dunlop et al.* [2005] this effect could be produced by either single-domain grain interactions or multidomain self-

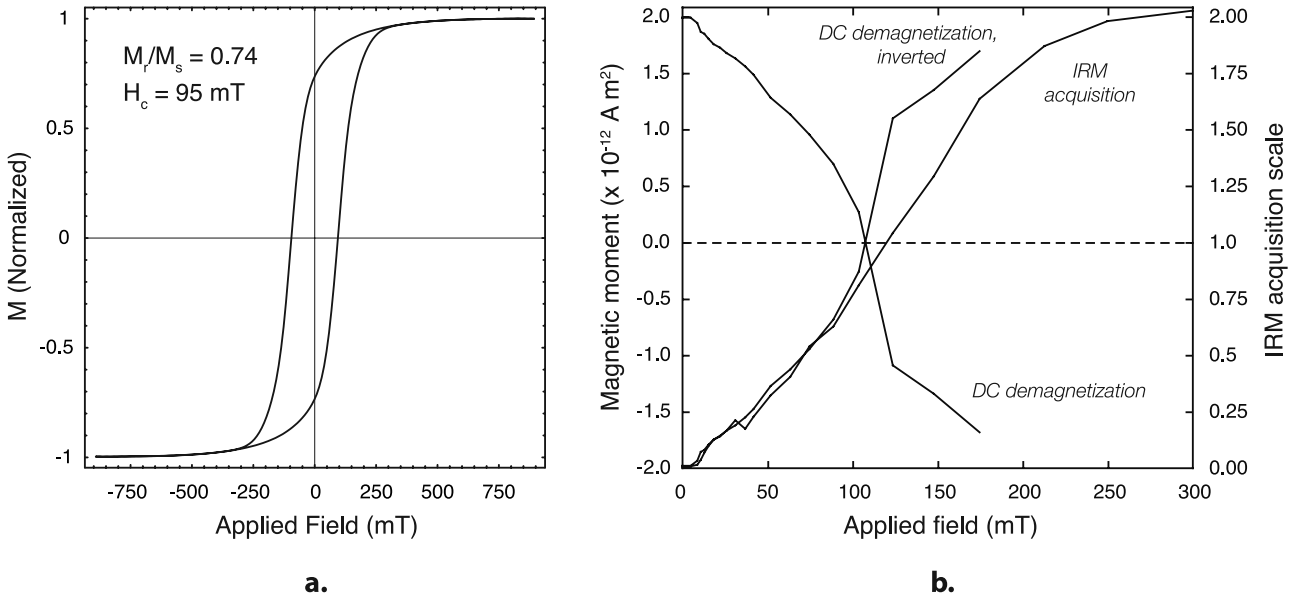

Figure 4. (a) Hysteresis loop of a single clinopyroxene crystal containing crystallographically oriented titanomagnetite inclusions. The loop was measured with the applied field parallel to the plane containing both inclusion elongation directions and perpendicular to the clinopyroxene c axis. (b) Coercivity spectra from isothermal acquisition and back-field demagnetization of a single clinopyroxene crystal. The spectra differ, indicating that remanence is more easily removed than it is gained. As *Dunlop et al.* [2005] point out, this difference could be due to single-domain interactions or to self-demagnetizing fields in multidomain material.

demagnetization. Here, the hard hysteresis properties suggest that single-domain grain interactions are responsible.

4.2. Electron Microscopy

4.2.1. Compositional Mapping

[9] Energy-selected imaging was used to create a color image of the iron, titanium and calcium distribution in a crystallographically oriented magnetite inclusion exsolved in clinopyroxene (Figure 2). Calcium (green) is limited to the clinopyroxene, and acts as a proxy for the edge of the inclusion. The box work texture in the inclusion results from magnetite and ulvöspinel unmixing. The blue regions are prisms of low-titanium magnetite, while the red bands are ulvöspinel lamellae, which have exsolved parallel to the {100} planes common to both phases. The average lengths and widths of the magnetite prisms are ~180 and ~50 nm, respectively, with an average aspect ratio of 0.34 (range 0.15–0.9) (Figure 5). Isolated crystals of these dimensions would exhibit single domain behavior [*Fabian et al.*, 1996]. In contrast to the well-studied magnetite-ulvöspinel intergrowths of the Mount Yamaska intrusion of Quebec [*Nickel*, 1958; *Evans and Wayman*, 1974; *Price*, 1980, 1982; *Harrison et al.*, 2002], the ulvöspinel lamellae in the Messum inclusions are wider in some directions than others, which may be a reflection of the stress regime inside the inclusion at the time of oxide unmixing. A similar geometric distribution of ulvöspinel lamellae was observed in a magnetite-ulvöspinel intergrowth from Taberg, Sweden [*Price*, 1979]. The variable thickness of the ulvöpsinel lamellae creates narrow stacks of closely spaced magnetite prisms. The geometry of these stacks will be shown to significantly influence the direction of magnetic remanence. The thickness of the sample shown in Figure 2 decreases from a maximum of ~125 nm at the lower left to ~50 nm at the upper right. These values were determined from t/λ_i maps obtained using energy-selected imaging [*Egerton*, 1996], where t is the specimen thickness and λ_i, the inelastic

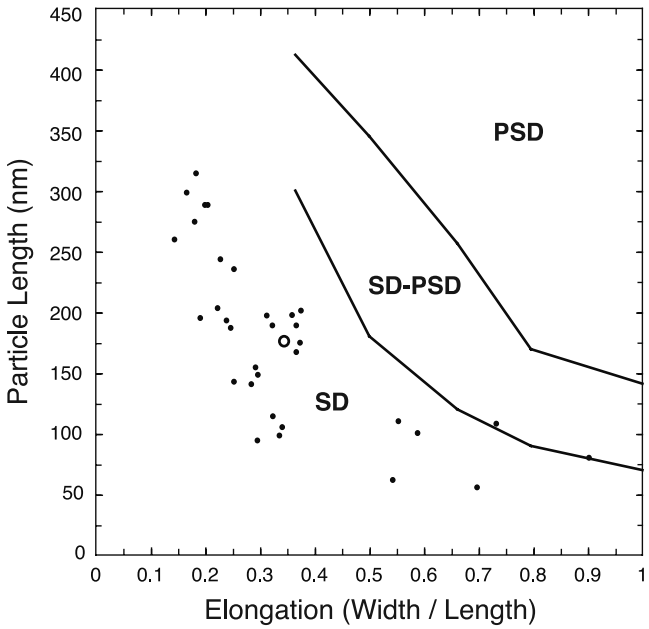

Figure 5. Distribution of magnetite prism dimensions. The open circle represents the average prism dimensions. Black lines denote single-domain (SD), single-domain/pseudosingle-domain (SD-PSD), and pseudosingle-domain (PSD) behavior as calculated for isolated grains by *Fabian et al.* [1996].

mean-free path for electrons in the sample, is estimated to be ~170 nm at 300 kV [*Harrison et al.*, 2002]. The surfaces of the TEM sample are expected to have sustained damage during ion beam thinning, creating magnetically dead layers. The magnetic thicknesses of the blocks are therefore lower than the measured sample thickness and can be estimated from the holographic phase shift across each block (see below). This approach provides an estimate for the average magnetic thickness of the sample of 20–30 nm.

4.2.2. Magnetic Induction Mapping

[10] The direction and magnitude of the measured in-plane magnetic induction are shown in Figure 6. The orientation and spacing of the black contours, which are generated from the magnetic contribution to the recorded holographic phase shift, provide the direction and the magnitude of the in-plane component of magnetic induction (projected in the incident beam direction). The positions of the magnetite blocks are outlined in white. The mean inner potential contribution to the phase shift has been removed using the procedure described by *Harrison et al.* [2002]. The magnitude of the measured induction increases where the contours are more closely spaced, while the direction is indicated both by the contours and by colors, according to the color wheel shown at the bottom of Figure 6. The contour spacing corresponds to a phase shift of 0.39 radians (22.3°) and a change in magnetic flux of 2.5×10^{-16} Wb. To help guide the eye, arrows have been added to each magnetite block to show the average direction of remanence. The resolution of the Lorentz lens used to collect the holographic images is 2 nm, but as a result of the signal-to-noise ratio of the holographic fringes and the slight smoothing used to minimize this noise, the spatial resolution of the magnetic information is estimated to be between 10 and 20 nm. In order to confirm the reproducibility of the remanence results, four IRM experiments were repeated (62.2 mT at ±30° and 2 T at ±30°). In all instances, fine details in the measured magnetic signal from one image are similar to those in the auxiliary material Figure S1.[1]

[11] A number of features confirm that the images in Figure 6 represent the magnetic flux inside the inclusion accurately: (1) The magnetic flux contours are most closely spaced within the magnetite blocks and more widely spaced within the nonmagnetic regions of the sample (clinopyroxene and ulvöspinel). (2) Changes in the directions of the contours correlate well with structural features in the inclusion, such as the positions of the thin ulvöspinel lamellae. (3) The general features of the inclusion's magnetic structure are identical (but reversed) for opposite directions of the applied field.

[12] One of the most striking observations is that the inclusion's average direction of remanence is not parallel to the external field direction (Figure 6). To examine the inclusion's complex magnetization, we begin by describing the remanent states of individual magnetite prisms and continue with observations of their collective interactions.

4.2.2.1. Magnetic Remanent States of Individual Prisms

[13] In Figure 6, individual prisms commonly display nonuniform single-domain magnetization states. The prisms are rarely magnetized parallel to their long axes (one exception is block A in Figure 6d). It is more common for the prisms to be magnetized at an angle to their long axes, suggesting that their shape anisotropy is not the dominant factor controlling remanent magnetization. There are occasional exceptions to this trend along the edge of the inclusion, where the magnetization may "wrap" or "curl" in such a way as to minimize the magnetostatic fringing field. The prisms around the edge of the inclusion are usually the first to reorient their magnetization directions between successive remanent measurements.

[14] The magnetization directions of smaller prisms are often determined by the direction of the return flux from larger nearby prisms. For example, block B (Figure 6a) is often magnetized antiparallel to the larger blocks immediately surrounding it. At room temperature, smaller magnetite prisms are closer to their blocking temperatures than larger single domain prisms, and therefore will require a smaller field to switch their magnetization. Thus the magnetization of the smaller blocks is more readily reoriented after each IRM treatment. Block B's dimensions ($30 \times 30 \times 40$ nm) are close to those of superparamagnetic grains described by *Dunlop and Özdemir* [1997] for magnetite at room temperature (25–30 nm for equidimensional grains). In isolation, some of these smaller prisms may behave superparamagnetically, but proximity to larger neighboring prisms helps stabilize their magnetization.

4.2.2.2. Collective Prism Behavior

[15] Since the separation of the magnetite blocks is much less than the dimensions of the blocks themselves, magnetostatic interactions play an important role in determining the collective behavior of the inclusion [*Muxworthy et al.*, 2003]. The measured flux contours often show little change when crossing the thinnest ulvöspinel walls (~20 nm). However, as the applied field approaches the coercivity of remanence, a "chevron" style of magnetic remanence is sometimes observed in adjacent prisms in the core of the inclusion (for example, see Figure 6j at 40.8 mT), suggesting a competition between the anisotropy of the individual magnetite prisms and the shape anisotropy of the stack. This chevron pattern is suggestive of a nonuniform reversal mechanism such as "buckling" or "fanning" [*Jacobs and Bean*, 1955; *Luborsky*, 1961]. The long, closely spaced stacks are typically magnetized along their diagonals, at a large angle to the direction of the applied field. In no instance is the average magnetization direction in the inclusion parallel to the long axes of the individual magnetite blocks.

[16] In some cases, several magnetite blocks form collective vortex "superstates" that minimize their magnetostatic energy [*Harrison et al.*, 2002]. The stray magnetic field emanating from the edge of the inclusion decreases when such superstates form. Unlike the vortex superstates seen in an earlier holography study on Mount Yamaska intergrowths [*Harrison et al.*, 2002], the multiprism vortices observed here are not always centered on ulvöspinel lamellae. Certain parts of the inclusion (e.g., at its lower left) are more prone to vortex formation than others. This behavior may result from the blocks in this region being thicker and slightly wider than others, or from their geometry at the corner of the inclusion. Other areas, such as that at the upper right of the inclusion, may be thin magnetically, leading to widely spaced contours. Sometimes chains

[1] Auxiliary materials are available in the HTML. doi:10.1029/2006JB004498.

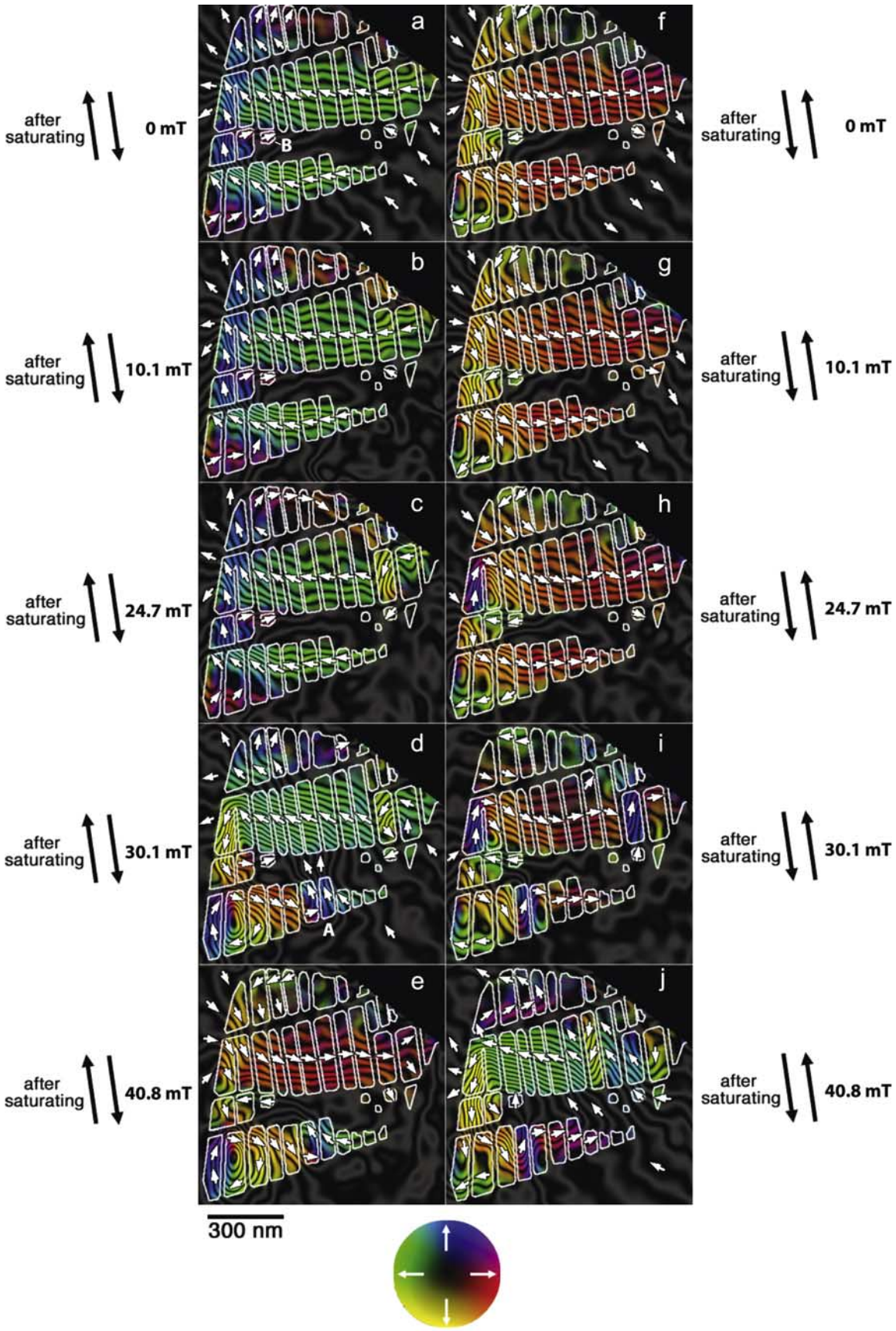

Figure 6. Magnetic induction maps showing magnetic remanent states in the inclusion of Figure 2. Each image was acquired after applying external fields, whose in-plane components are indicated. The direction of the magnetic flux is shown using contours, colors, and arrows.

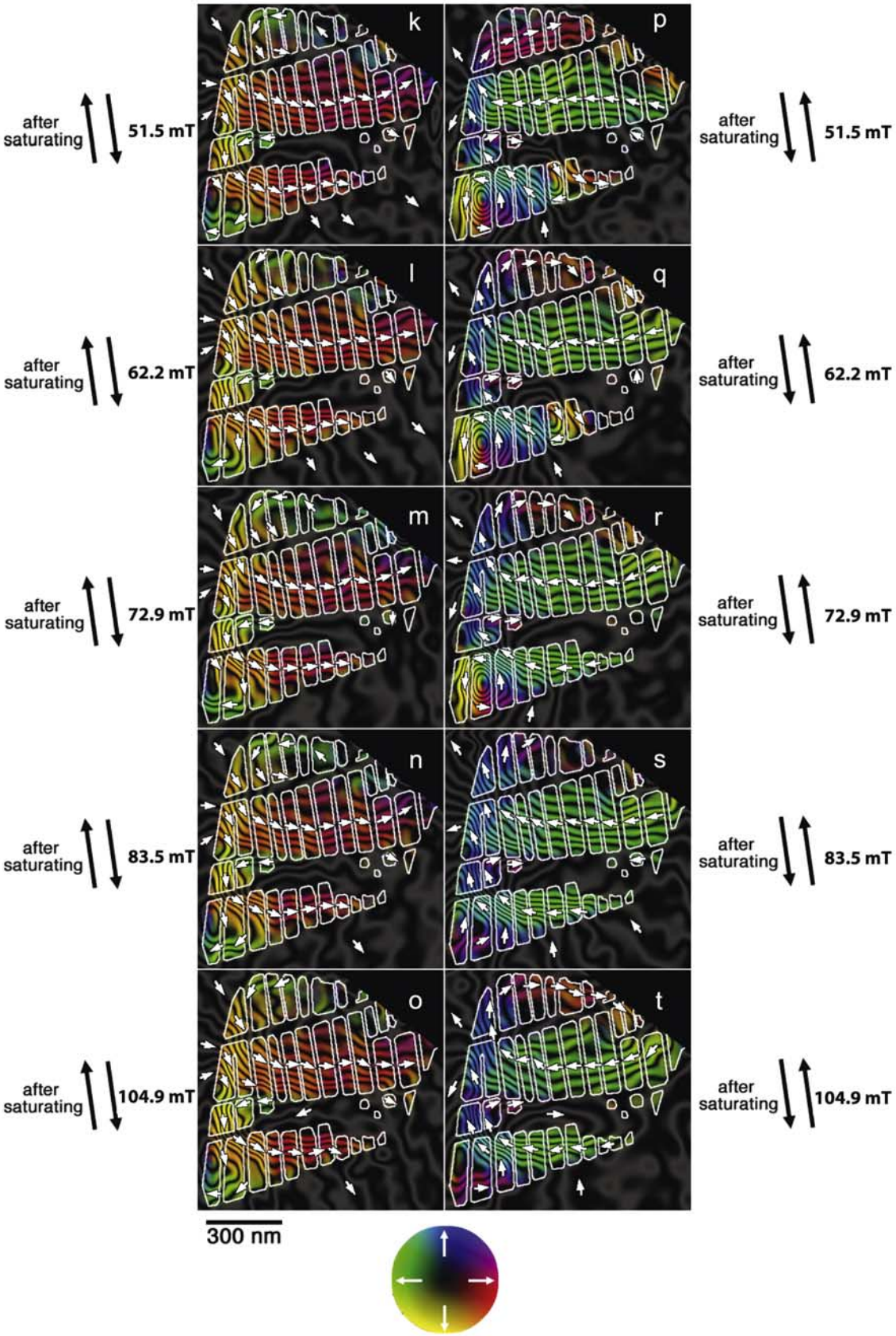

Figure 6. (continued)

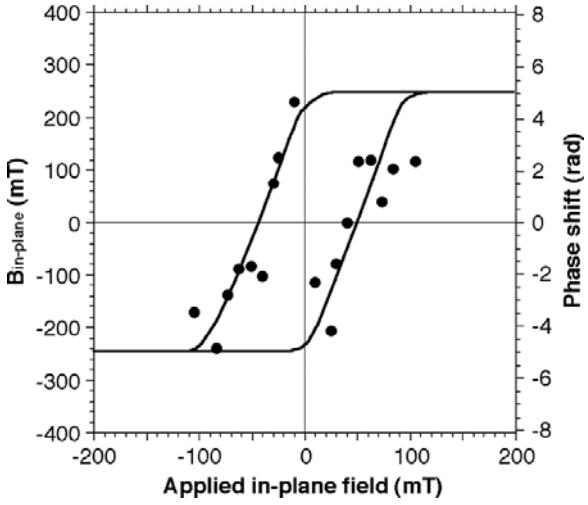

Figure 7. Coercivity of remanence measured from the images shown in Figure 6, in the region indicated by a dashed line in Figure 2. The in-plane magnetization (in mT) was calculated from the phase shift (in radians) on the assumption that the magnetic thickness of the sample was 20 nm.

of vortices form along a stack of closely spaced magnetite blocks.

[17] It is particularly noteworthy that different regions of the inclusion reverse at different applied fields. For example, the large stack of closely spaced prisms making up the core of the inclusion reverses between 30 and 50 mT, while the surrounding prisms making up its edge reverse at smaller fields. Thus a single inclusion has a spectrum of coercivities.

[18] The complexity of the magnetic domain states in the inclusion increases as the coercivity of remanence (H_{CR}) is approached. Multiprism vortex states become more common as H_{CR} is approached, and more rare after it has passed. Owing to the wide variation in the resulting magnetization directions, the total remanence (M_R) of the inclusion decreases close to the coercivity of remanence. By measuring the average step in the magnetic contribution to the phase shift across the inclusion parallel to the applied IRM (approximately proportional to the magnetic moment of the inclusion), it is possible to use electron holography to construct a ''remanence hysteresis'' loop from a chosen region of the inclusion [*Harrison et al.*, 2002]. The part of the inclusion outlined by a dashed box in Figure 2 was used to generate the hysteresis loop shown in Figure 7, which suggests a value for the coercivity of remanence of ~50 mT. This value is lower than H_{CR} values obtained from back-field demagnetization experiments on single crystals of clinopyroxene. However, these values are not directly comparable as the back-field demagnetization experiments measure H_{CR} from the three-dimensional needle-shaped magnetite-ulvöspinel assemblages, while the electron holography experiments in this study measure H_{CR} from a one-prism-thick cross section through an inclusion.

4.3. Directionally Varied Isothermal Remanent Magnetization Measurements

[19] In a separate but related experiment, the macroscopic behavior of clinopyroxene fragments was observed to reflect the influence of both the needle-like shape of the inclusions and the microstructures within them. Single fragments of clinopyroxene were mounted onto quartz slides, with the $(010)_{cli}$ plane containing the inclusions oriented parallel to the slide surface. Seventy-two 1.1 T IRMs were imparted to the clinopyroxene in 5° azimuthal steps, covering one full 360° rotation of the fragment. The resulting magnetization direction after each step is plotted in Figure 8 for one such fragment. The data cluster at four distinct azimuthal angles: ~145°, ~175°, ~325°, and ~355°. The clusters at ~175° and ~355° are subparallel to the elongation direction of the Z inclusions, which are subparallel to the clinopyroxene *c* axis [*Bown and Gay*, 1959; *Fleet et al.*, 1980]. The clusters at ~145° and 325° are subparallel to the orientation of the [00−1] and [001] directions of the titanomagnetite inclusions. Two microstructural features could be responsible for these particular orientations of data clusters: the elongation direction of the prism stacks, and/or the elongation direction of the prisms themselves. The clinopyroxene fragment used in this experiment had abundant Z inclusions and very rare X inclusions, which explains why few of the data cluster parallel to the *a* axis of the clinopyroxene. The remanence directions are distributed between the elongation direction of the Z inclusions and the elongation direction of the stacks of closely spaced prisms. Thus the overall remanence carried by the clinopyroxene crystal is affected by the elongation of both the magnetite inclusions and the magnetite prism stacks within them.

[20] The difference between the orientation of the applied field and the direction of remanence in the experiments described above is shown in Figure 9a and varies from 20° to 80°. Normalized intensity as a function of applied field orientation is shown in Figure 9b, and varies from 25% to 100%. Much of the variation in Figure 9 is due to the orientation of the inclusions' long axes. However, particular details of the remanence response (indicated by arrows) cannot be attributed to the inclusions' elongation. We believe these features are related to the magnetite-ulvöspinel microstructure with the inclusions. The variation in remanence direction and intensity shown in Figure 9 only describes anisotropy over a single plane. The full three-dimensional remanence anisotropy of single crystals containing exsolved inclusions will be described in future work, but this example demonstrates that a single crystal's remanence is influenced by both the elongation of the inclusion and the magnetite-ulvöspinel exsolution texture within it.

5. Discussion

[21] The magnetic induction maps measured using off-axis electron holography show that the magnetization in the magnetite-ulvöspinel assemblage is complex and highly nonuniform. The most important observation is that the magnetic moment of the inclusion is controlled primarily by the shape anisotropy of prism stacks, rather than by the shape anisotropy of the individual magnetite prisms. The final remanence state of an inclusion is a balance between competing anisotropy energies (Figure 10) including: magnetocrystalline anisotropy, the shape anisotropies of individual magnetite prisms, the shape anisotropy of a stack of

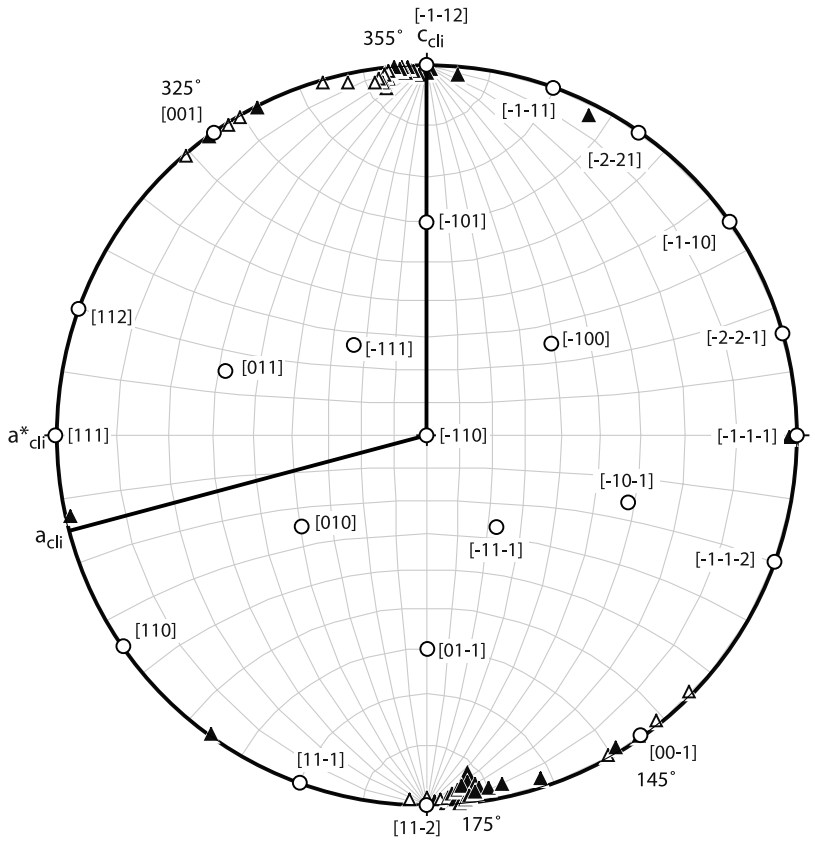

Figure 8. Equal-angle plot of remanence directions (triangles) from an oriented clinopyroxene fragment. Open (solid) triangles represent upper (lower) hemisphere. Circles denote magnetite crystallographic axes projected onto the upper hemisphere. Bold lines represent the orientation of the clinopyroxene *a* and *c* axes. Labeled circles represent the orientations of magnetite axes within the clinopyroxene and are taken from *Feinberg et al.* [2004].

closely spaced magnetite prisms, and the overall shape anisotropy of the inclusion as a whole. In the present TEM sample, the prism stacks played a particularly strong role in determining the overall magnetization direction of the inclusion. In contrast, magnetocrystalline anisotropy energy (E_k), which is minimized along $\langle 111 \rangle$ in magnetite ($K_1 = -1.35 \times 10^4$ J/m^3 and $K_2 = -0.28 \times 10^4$ J/m^3 [*Dunlop and Özdemir*, 1997]), plays the least important role. When the inclusions are viewed as needle-shaped three-dimensional assemblages of interacting prisms (as opposed to thinned, one prism-thick TEM specimens), the role of shape anisotropy of the entire oxide inclusion may increase. Directional data gathered during alternating field and thermal demagnetization experiments, as well as IRM acquisition data (e.g., Figure 8), show that the remanence directions of single crystals of magnetite-bearing clinopyroxene occur solely within the $(010)_{cli}$ plane that contains both sets of inclusions, confirming the fact that shape anisotropy of the overall inclusion is an important, if not dominant, factor. Future electron holography studies on TEM specimens prepared parallel to the long axes of the inclusions will help to quantify the effect of an assemblage's shape anisotropy on the final remanence.

[22] The observation that clinopyroxene-hosted inclusions, both with and without internal microtextures, always record directions in the $(010)_{cli}$ plane is critically important to their use in paleomagnetic studies. Single crystals of inclusion-bearing clinopyroxene will consistently exhibit an anisotropy of direction and intensity. A bulk rock sample containing silicate-hosted inclusions will have a remanence direction that reflects both the rock's mineral fabric and the remanence of other discrete magnetic oxides and sulphides. If a bulk rock sample contains a population of randomly oriented clinopyroxene grains, then this anisotropy will not prevent the use of standard paleomagnetic techniques. However, if clinopyroxene crystals in a paleomagnetic sample exhibit a preferred orientation, then the magnetic remanence of the bulk sample will be biased and require correction [*Selkin et al.*, 2000].

[23] The magnetic induction maps presented in this study, and the magnetic force microscope images of *Feinberg et al.* [2005], show that the interiors of finely exsolved inclusions are composed of magnetite prisms that have widely varying magnetic directions. This distribution of directions within a single inclusion is important for the use of such materials as recorders of the intensity of the Earth's ancient magnetic field. Magnetic interactions between magnetite prisms decrease the overall intensity recorded by an inclusion. It is as yet unclear how the strength of a magnetizing field influences the level of interactions within

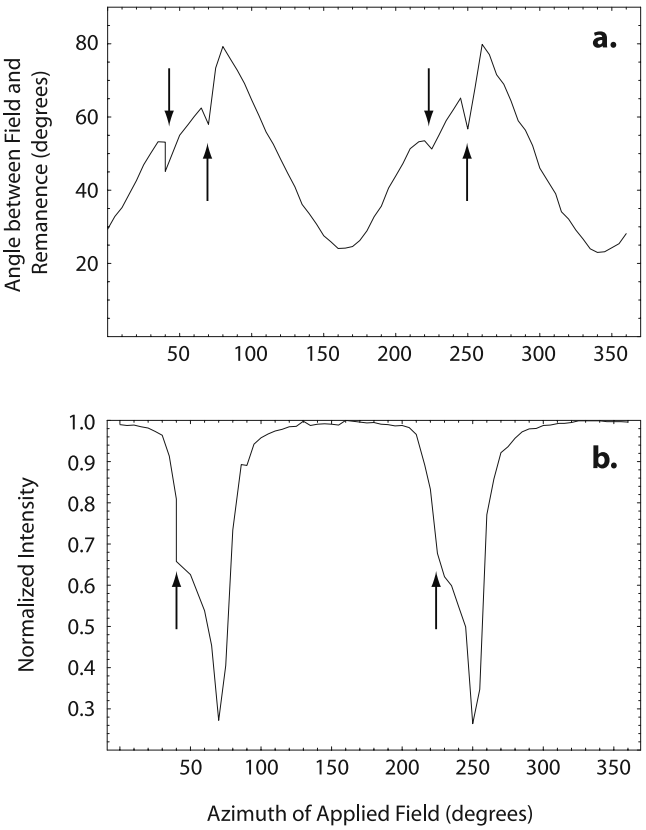

Figure 9. Remanence (a) direction and (b) intensity as function of azimuth of applied field for a single clinopyroxene crystal containing finely exsolved magnetite-ulvöspinel inclusions. The 1.1 T IRMs were imparted in 5° steps. Arrows indicate details in the remanence response repeated every 180° which we attribute to magnetite-ulvöspinel exsolution.

an assemblage of magnetite prisms as a sample is cooled through its blocking temperature. Future experimental and micromagnetic modeling studies will help to elucidate the role of prism interactions during magnetization under different field strengths.

[24] It is important to stress that these magnetic inclusions are crystallographically exsolved within their hosts. Over 40 years of data from electron backscatter diffraction, TEM selected area diffraction, and X-ray diffraction experiments [*Feinberg et al.*, 2004, and references therein] indicate that the orientation relationships between the titanomagnetite and silicate crystal lattices are identical within all clinopyroxene crystals. By extension, the orientation of the ulvöspinel lamellae in finely exsolved oxide inclusions is also identical within all clinopyroxene crystals. Thus we expect the interplay of anisotropy energies observed in our samples to be present in all finely exsolved silicate-hosted inclusions. This consistency greatly simplifies the remaining questions about the inclusions' remanence acquisition. Answers to these questions will allow the inclusions to be used widely in paleomagnetic applications, such as expanding the geomagnetic polarity timescale into the Paleozoic and Precambrian, or compiling paleointensity records.

6. Conclusions

[25] The distribution of magnetic domain states in finely exsolved oxide inclusions in clinopyroxene is highly nonuniform. Mineralogical features such as the thicknesses of ulvöspinel lamellae exert a strong influence on the magnetic structure within each inclusion. Closely spaced magnetite prisms show a high level of magnetostatic interaction, either as long columns or as multipart vortex states. This collective magnetic behavior can be strong enough to dominate over both the shape and the magnetocrystalline anisotropies of individual prisms. Consequently, the final remanence direction may appear at a large angle to the magnetizing field, and is a reflection of the inclusion's mineralogic microstructure. If a paleomagnetic sample contains a random distribution of numerous clinopyroxene grains, then this extreme magnetic anisotropy is avoided. However, if the clinopyroxene within a paleomagnetic sample exhibits a preferred orientation, as is common in cumulates and some mafic dikes, then magnetic anisotropy will bias the final remanence direction and require a correction. The key to understanding the magnetic structures within finely exsolved inclusions is to understand the processes that form their nanometer-scale mineralogic structures. As our knowledge of these processes improves, so the crystallographic consistency inherent to exsolved inclusions will ultimately allow paleomagnetists to use these inclusions as dependable and abundant sources of information about the direction and intensity of the Earth's ancient magnetic field.

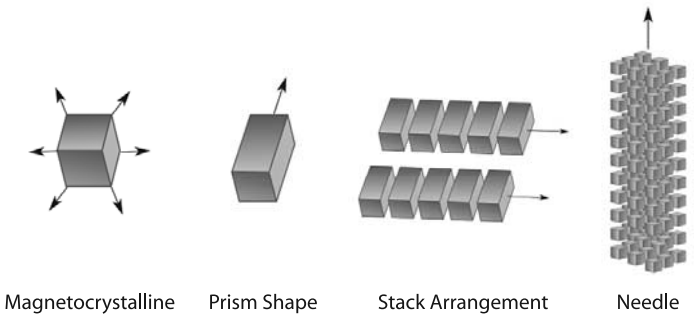

Figure 10. Schematic diagram illustrating the competing anisotropy energies in assemblages of finely exsolved magnetite and ulvöspinel.

[26] **Acknowledgments.** The authors would like to thank E. T. Simpson for assistance and discussions. J.M.F., G.R.S., and P.R.R. were supported through National Science Foundation grants EAR-0236925, and EAR-0309686, J.M.F. through an Institute for Rock Magnetism Visiting Fellowship and NERC (NE/C518422/1), R.J.H. through NERC (NE/B501339/1), and R.D.B. through the Royal Society. J.M.F. is also grateful to K. Verosub and C. Pike for access to the AGM at the University of California, Davis. We thank Ted Evans, Suzanne McEnroe, and an anonymous referee for helpful reviews that greatly improved the paper.

References

Akimoto, S. (1962), Magnetic properties of FeO-Fe_2O_3-TiO_2 system as a basis of rock magnetism, *J. Phys. Soc. Jpn.*, *17*, suppl. B1, 706–710.

Bogue, S. W., S. Gromme, and J. W. Hillhouse (1995), Paleomagnetism, magnetic anisotropy, and mid-Cretaceous paleolatitude of the Duke Island (Alaska) ultramafic complex, *Tectonics*, *14*, 1133–1152.

Bown, M. G., and P. Gay (1959), The identification of oriented inclusions in pyroxene crystals, *Am. Mineral.*, *44*, 592–602.

Cottrell, R. D., and J. A. Tarduno (1999), Geomagnetic paleointensity derived from single plagioclase crystals, *Earth Planet. Sci. Lett.*, *169*, 1–5.

Cottrell, R. D., and J. A. Tarduno (2000), In search of high-fidelity geomagnetic paleointensities: A comparison of single plagioclase crystal and whole rock Thellier-Thellier analyses, *J. Geophys. Res.*, *105*, 23,579–23,594.

Davis, K. E. (1981), Magnetite rods in plagioclase as the primary carrier of stable NRM in ocean floor gabbros, *Earth Planet. Sci. Lett.*, *55*, 190–198.

Dunin-Borkowski, R. E., M. R. McCartney, and D. J. Smith (2004), Electron holography of nanostructured materials, in *Encyclopedia of Nanoscience and Nanotechnology*, edited by H. S. Nalwa, pp. 41–99, Am. Sci., Stevenson Ranch, Calif.

Dunlop, D. J. (1986), Coercive forces and coercivity spectra of submicron magnetites, *Earth Planet. Sci. Lett.*, *78*, 288–295.

Dunlop, D. J., and O. Özdemir (1997), *Rock Magnetism: Fundamentals and Frontiers*, 1st ed., 573 pp., Cambridge Univ. Press, New York.

Dunlop, D. J., B. Zhang, and Ö. Özdemir (2005), Linear and nonlinear Thellier paleointensity behavior of natural minerals, *J. Geophys. Res.*, *110*, B01103, doi:10.1029/2004JB003095.

Egerton, R. F. (1996), *Electron Energy-Loss Spectroscopy in the Electron Microscope*, 2nd ed., Springer, New York.

Evans, M. E., and M. W. McElhinny (1966), The paleomagnetism of the Modipe Gabbro, *J. Geophys. Res.*, *71*, 6053–6063.

Evans, M. E., and M. L. Wayman (1974), An investigation of the role of ultra-fine titanomagnetite intergrowths in paleomagnetism, *Geophys. J. R. Astron. Soc.*, *36*, 1–10.

Evans, M. E., M. W. McElhinny, and A. C. Gifford (1968), Single domain magnetite and high coercivities in a gabbroic intrusion, *Earth Planet. Sci. Lett.*, *4*, 142–146.

Evans, M. E., D. Krása, W. Williams, and M. Winklhofer (2006), Magnetostatic interactions in a natural magnetite-ulvöspinel system, *J. Geophys. Res.*, *111*, B12S16, doi:10.1029/2006JB004454.

Fabian, K., A. Kirchner, W. Williams, F. Heider, T. Leibl, and A. Huber (1996), Three-dimensional micromagnetic calculations for magnetite using FFT, *Geophys. J. Int.*, *124*, 89–104.

Feinberg, J. M., H.-R. Wenk, P. R. Renne, and G. R. Scott (2004), Epitaxial relationships of clinopyroxene-hosted magnetite determined using electron backscatter diffraction (EBSD) technique, *Am. Mineral.*, *89*, 462–466.

Feinberg, J. M., G. R. Scott, P. R. Renne, and H.-R. Wenk (2005), Exsolved magnetite inclusions in silicates: Features determining their remanence behavior, *Geology*, *33*, 513–516.

Fleet, M. E., G. A. Bilcox, and R. L. Barnett (1980), Oriented magnetite inclusions in pyroxenes from the Grenville Province, *Can. Mineral.*, *18*, 89–99.

Golla, U., and A. Putnis (2001), Valence state mapping and quantitative electron spectroscopic imaging of exsolution in titanohematite by energy-filtered TEM, *Phys. Chem. Miner.*, *28*, 119–129.

Halls, H. C., and B. X. Zhang (1995), Tectonic implications of clouded feldspar in Proterozoic mafic dyke swarms, in *Dyke Swarms of Peninsular India*, edited by T. C. Devaraju, pp. 65–80, Geol. Soc. of India, Bangalore.

Hargraves, R. B., and W. M. Young (1969), Source of stable remanent magnetism in Lambertville diabase, *Am. J. Sci.*, *267*, 1161–1177.

Hargraves, R. B., J. C. Briden, and B. A. Daniels (1999), Palaeomagnetism and magnetic fabric in the Freetown Complex, Sierra Leone, *Geophys. J. Int.*, *136*, 705–713.

Harrison, R. J., R. E. Dunin-Borkowski, and A. Putnis (2002), Direct imaging of nanoscale magnetic interactions in minerals, *Proc. Natl. Acad. Sci. U.S.A.*, *99*, 16,556–16,561.

Hattingh, P. J. (1986a), The paleomagnetism of the main zone in the western Bushveld Complex, *Earth Planet. Sci. Lett.*, *79*, 441–452.

Hattingh, P. J. (1986b), The paleomagnetism of the main zone of the eastern Bushveld Complex, *Tectonophysics*, *124*, 271–295.

Hattingh, P. J. (1989), Paleomagnetism of the upper zone of the Bushveld Complex, *Tectonophysics*, *165*, 131–142.

Jacobs, I. S., and C. P. Bean (1955), Approach to elongated fine-particle magnets, *Phys. Rev.*, *100*, 1060–1067.

Luborsky, F. E. (1961), High coercive materials—Development of elongated particle magnets, *J. Appl. Phys.*, *32*, 171S–183S.

Moskowitz, B. M. (1981), Methods for estimating the Curie temperatures of titanomaghemites from experimental J_s-T data, *Earth Planet. Sci. Lett.*, *53*, 84–88.

Murthy, G. S., M. E. Evans, and D. I. Gough (1971), Evidence of single-domain magnetite in Michikamau anorthosite, *Can. J. Earth Sci.*, *8*, 361–370.

Muxworthy, A., W. Williams, and D. Virdee (2003), Effect of magnetostatic interactions on the hysteresis parameters of single-domain and pseudo-single-domain grains, *J. Geophys. Res.*, *108*(B11), 2517, doi:10.1029/2003JB002588.

Nickel, E. H. (1958), The composition and microtexture of an ulvöspinel-magnetite intergrowth, *Can. Mineral.*, *6*, 191–199.

Price, G. D. (1979), Microstructures in titanomagnetites as guides to cooling rates of a Swedish intrusion, *Geol. Mag.*, *116*, 313–318.

Price, G. D. (1980), Exsolution microstructures in titanomagnetites and their magnetic significance, *Phys. Earth Planet. Inter.*, *23*, 2–12.

Price, G. D. (1982), Exsolution in titanomagnetites as an indicator of cooling rates, *Mineral. Mag.*, *46*, 19–25.

Renne, P. R., and T. C. Onstott (1988), Laser selective demagnetization: Application of a new technique in rock magnetism and paleomagnetism, *Science*, *242*, 1152–1155.

Renne, P. R., G. R. Scott, J. M. G. Glen, and J. M. Feinberg (2002), Oriented inclusions of magnetite in clinopyroxene: Source of stable remanent magnetization in gabbros of the Messum Complex, Namibia, *Geochem. Geophys. Geosyst.*, *3*(12), 1079, doi:10.1029/2002GC000319.

Schlinger, C. M., and D. R. Veblen (1989), Magnetism and transmission electron microscopy of Fe-Ti oxides and pyroxenes in a granulite from Lofoten, Norway, *J. Geophys. Res.*, *94*, 14,009–14,026.

Scofield, N., and W. M. Roggenthen (1986), Petrologic evolution of plagioclase-rich cumulates from the Wichita Mountains, Oklahoma: Effects upon magnetic remanence properties, *Geology*, *14*, 908–911.

Selkin, P. A., J. S. Gee, L. Tauxe, W. P. Meurer, and A. J. Newell (2000), The effect of remanence anisotropy on paleointensity estimates: A case study from the Archean Stillwater Complex, *Earth Planet. Sci. Lett.*, *183*, 403–416.

Smirnov, A. V., J. A. Tarduno, and B. N. Pisakin (2003), Paleointensity of the early geodynamo (2.45 Ga) as recorded in Karelia: A single-crystal approach, *Geology*, *31*, 415–418.

Tarduno, J. A., and R. D. Cottrell (2005), Dipole strength and variation of the time-averaged reversing and nonreversing geodynamo based on Thellier analyses of single plagioclase crystals, *J. Geophys. Res.*, *110*, B11101, doi:10.1029/2005JB003970.

Tarduno, J. A., R. D. Cottrell, and A. V. Smirnov (2001), High geomagnetic intensity during the mid-Cretaceous from Thellier analyses of single plagioclase crystals, *Science*, *291*, 1779–1783.

Tarduno, J. A., R. D. Cottrell, and A. V. Smirnov (2002), The Cretaceous superchron geodynamo: Observations near the tangent cylinder, *Proc. Natl. Acad. Sci. U.S.A.*, *99*, 14,020–14,025.

Tauxe, L. (1998), *Paleomagnetic Principles and Practice,* 1st ed., p. 299, Springer, New York.

Tonomura, A. (1992), Electron-holographic interference microscopy, *Adv. Phys.*, *41*, 59–103.

Völkl, E., L. F. Allard, and D. C. Joy (Eds.) (1998), *Introduction to Electron Holography*, Springer, New York.

Wu, Y. T., M. Fuller, and V. A. Schmidt (1974), Microanalysis of NRM in a granodiorite intrusion, *Earth Planet. Sci. Lett.*, *23*, 275–285.

Xu, W., J. Geissman, R. van der Voo, and D. Peacor (1997), Electron microscopy of iron oxides and implications for the origin of magnetizations and rock magnetic properties of banded series rocks of the Stillwater Complex, Montana, *J. Geophys. Res.*, *102*, 12,139–112,157.

Yu, Y., and D. J. Dunlop (2001), Paleointensity determination on the Late Precambrian Tudor Gabbro, Ontario, *J. Geophys. Res.*, *106*, 26,331–326,343.

R. E. Dunin-Borkowski, Department of Materials Science and Metallurgy, University of Cambridge, Pembroke Street, Cambridge CB2 3QZ, UK.

J. M. Feinberg and R. J. Harrison, Department of Earth Sciences, University of Cambridge, Downing Street, Cambridge CB2 3EQ, UK. (jfei05@esc.cam.ac.uk)

T. Kasama, Frontier Research System, Institute of Physical and Chemical Research, Hatoyama, Saitama 350-0395, Japan.

P. R. Renne, Department of Earth and Planetary Science, University of California, 340 McCone Hall, Berkeley, CA 94720, USA.

G. R. Scott, Berkeley Geochronology Center, 2455 Ridge Road, Berkeley, CA 94709, USA.